Fiducial Reference Measurements for Satellite Ocean Colour Phase-2

Guidelines for individual OCR full characterisation and calibration

FRM4SOC2-D8

Title	TR: Guidelines for individual OCR full characterisation and calibration
Document reference	FRM4SOC2-D8
Project	EUMETSAT – FRM4SOC Phase-2
Contract	EUMETSAT Contract No. EUM/CO/21/460002539/JIG
Deliverable	D-8
Version	3.1
Date issued	26.04.2023

Prepared By	Approved by
Name: Viktor Vabson	Name: Juan Ignacio Gossn
Organisation: UT	Organisation: EUMETSAT
Position: FRM4SOC Phase 2 Task 4 Leader	Position: FRM4SOC Phase 2 Technical Officer
Date: 26.04.2023	Date:
Signature:	Signature: Juan Ignacio Gossn Digitally signed by Juan Ignacio Gossn Date: 2023.05.15 14:54:04 +02'00'

Fiducial Reference Measurements for Satellite Ocean Colour Phase-2

TR: *Guidelines for individual OCR full characterisation and calibration* (FRM4SOC2-D8)

TECHNICAL REPORT

Viktor Vabson, Ilmar Ansko, Riho Vendt, Joel Kuusk

UNIVERSITY OF TARTU
Tartu Observatory

2023

PROGRAMME OF THE EUROPEAN UNION

opernicus Europe's eyes on Earth

IMPLEMENTED BY EUMETSAT

Document Control Table

Title	TR: Guidelines for individual OCR full characterisation and calibration
Document reference	FRM4SOC2-D8
Project	EUMETSAT – FRM4SOC Phase-2
Contract	EUMETSAT Contract No. EUM/CO/21/460002539/JIG
Deliverable	D-8
Version	3.1
Date Issued	26.04.2023

Document Change Record

Index	Issue	Revision	Date	Brief description	Issued by
1	1	0	20.04.2022	Original version	V. Vabson
2	2	0	12.07.2022	Updates after EUMETSAT review	V. Vabson
3	2	1	14.10.2022	Updates after ERB review	V. Vabson
4	3	0	10.02.2023	Updates after PM7 review	V. Vabson
5	3	1	26.04.2023	Release for publication	V. Vabson

Distribution List

Public at https://frm4soc2.eumetsat.int

Acronyms and Abbreviations

Acronym	Description
AAOT	Acqua Alta Oceanographic Tower
AERONET-OC	The Ocean Color component of the Aerosol Robotic Network
AMT	Atlantic Meridional Transect
BRDF	Bidirectional reflectance distribution function
Cal	Calibration
CCPR	Consultative Committee for Photometry and Radiometry
CEOS	Committee on Earth Observation Satellites
Char	Characterization
CIPM	Comité International des Poids et Mesures (International Committee for Weights and Measures)
CIMP MRA	CIPM Mutual Recognition Arrangement
EO	Earth Observation
ESA	European Space Agency
EUMETSAT	European Organisation for the Exploitation of Meteorological Satellites
FICE	Fiducial Inter-Comparison Experiment
FOV	Field of view
FRM	Fiducial Reference Measurements
FRMOCnet	Copernicus FRM-certified OC instrument network
FRM4SOC	Fiducial Reference Measurements for Satellite Ocean Colour
FWHM	Full Width at Half Maximum
GEO	Group on Earth Observations
ILAC	International Laboratory Accreditation Cooperation
IOCCG	International Ocean-Colour Coordinating Group
LUT	Look Up Table
MERIS	Medium Resolution Imaging Spectrometer
MVT	MERIS Validation Team
NASA	National Aeronautics and Space Administration
NERC	Natural Environment Research Council
NMI	National Metrology Institute
NPL	National Physical Laboratory
OC	Ocean Colour
OCDB	Ocean Colour Database
OCR	Ocean Colour Radiometer
QA	Quality Assurance
QA4EO	Quality Assurance framework for Earth Observation
QC	Quality Control
QTH	Quartz tungsten halogen
ROI	Return On Investment
RSP	Remote Sensing and Products Division
RD	Reference Document
S3	Sentinel-3
S3VT-OC	Sentinel-3 Validation Team – Ocean Colour group
SeaWiFS	Sea-Viewing Wide Field-of-View Sensor
SIRREX	SeaWiFS Intercalibration Round Robin Experiments
SI	International System of Units
SOW	Statement of Work
SST	Sea Surface Temperature
TO	Tartu Observatory, University of Tartu
TR	Technical Report
UT	University of Tartu

Acronym	Description
VAL	Validation
VIM	Vocabulaire International de Métrologie (International Vocabulary in Metrology)

Contents

Applicable documents

ID	Description
[AD-0]	Statement of Work for FRM4SOC phase2, EUM/RSP/SOW/19/1131157
[AD-1]	ESA's contract no 4000117454/16/I-SBo (https://frm4soc.org)
[AD-2]	D-70: Technical Report TR-2 "A Review of Commonly used Fiducial Reference Measurement (FRM) Ocean Colour Radiometers (OCR) used for Satellite OCR Validation" (available at https://frm4soc.org/index.php/documents/deliverables/)
[AD-3]	'Statement of Work for Database of Ocean Colour In Situ Fiducial Reference Measurement Collections for Calibration and Validation', EUM/OPSCOPER/SOW/17/956607.
[AD-4]	IOCCG Protocol Series (2019). "Protocols for Satellite Ocean Colour Data Validation: In Situ Optical Radiometry". Zibordi, G., Voss, K. J., Johnson, B. C. and Mueller, J. L. IOCCG Ocean Optics and Biogeochemistry Protocols for Satellite Ocean Colour Sensor Validation, Volume 3.0, IOCCG, Dartmouth, NS, Canada. (Available at https://ioccg.org/what-we-do/ioccg-publications/oceanoptics-protocols-satellite-ocean-colour-sensor-validation/)
[AD-5]	K. Ruddick et. al., "A Review of Protocols for Fiducial Reference Measurements of Water-Leaving Radiance for Validation of Satellite Remote-Sensing Data over Water", Remote Sens. 2019, 11(19), 2198; https://doi.org/10.3390/rs11192198
[AD-6]	K. Ruddick et. al., "A Review of Protocols for Fiducial Reference Measurements of Downwelling Irradiance for the Validation of Satellite Remote Sensing Data over Water", Remote Sens. 2019, 11(15), 1742; https://doi.org/10.3390/rs11151742
[AD-7]	International Network for Sensor Inter-comparison and Uncertainty assessment for Ocean Color Radiometry (INSITU-OCR), http://ioccg.org/wpcontent/uploads/2016/02/INSITU-OCR-white-paper.pdf.
[AD-8]	D-80a: Technical Report TR-3a "Protocols and Procedures to Verify the Performance of Reference Irradiance Sources used by Fiducial Reference Measurement Ocean Colour Radiometers for Satellite Validation" (available at https://frm4soc.org/index.php/documents/deliverables/)
[AD-9]	D-80b Technical Report TR-3b "Protocols and Procedures to Verify the Performance of Reference Radiance Sources used by Fiducial Reference Measurement Ocean Colour Radiometers for Satellite Validation" (available at https://frm4soc.org/index.php/documents/deliverables/)
[AD-10]	Białek, A.; Douglas, S.; Kuusk, J.; Ansko, I.; Vabson, V.; Vendt, R.; Casal, A.T. Example of Monte Carlo Method Uncertainty Evaluation for Above-Water Ocean Colour Radiometry. Remote Sens. 2020, 12, 780. https://doi.org/10.3390/rs12050780
[AD-11]	TR-9 Technical Report "Results from the First FRM4SOC Field Inter-Comparison Experiment (FICE) of Ocean Colour Radiometers" (available at https://frm4soc.org/index.php/documents/deliverables/)
[AD-12]	IOCCG Ocean Optics & Biogeochemistry Protocols for Satellite Ocean Colour Sensor Validation (https://ioccg.org/what-we-do/ioccg-publications/ocean-opticsprotocols-satellite-ocean-colour-sensor-validation/)

Reference documents

ID	Description
[RD-1]	ESA's contract no 4000117454/16/I-SBo (https://frm4soc.org)

1 Scope

The current document is the Technical Report about guidelines defined for the complete characterisation and SI-traceable calibration of single instruments from the selected OCR models as required by the terms of the Invitation To Tender (ITT) No. 20/220036 "Copernicus – Fiducial Reference Measurements for Satellite Ocean Colour (FRM4SOC phase-2) issued by EUMETSAT. Guidelines shall be followed by laboratories active in the field of cal/char of OCRs. In preparation of this document, the Strategy plan for the secondary laboratory cal/char inter-comparison exercise and the definition and harmonisation of laboratory guidelines D-11, documents D-2, D-7 and D-12 are followed. This document forms deliverable D-8 of the FRM4SOC phase-2 project.

The main aim of this deliverable is to define general guidelines for the full characterisation and calibration of single instruments from selected OCR instrument types serving as methodical aid for FRM measurement scientists/teams and secondary (especially beginning) laboratories active in the calibration and characterisation of OCR. In this document, the guidelines [1], [2], requirements of the document D-2, and results of repeated characterisations and calibrations of two RAMSES and two HyperOCR sensors presented in D-7, are carefully reviewed and accounted for.

From the analysis of requirements of the document D-2, and from the results of repeated characterisations and calibrations, a characterisation routine for single instruments from FRMOCnet OCR selected models is proposed.

2 Compatibility

Table 2-1. Compatibility

No.	Requirement
1.	SOW- Req. 31: Guidelines shall be defined for full characterisation and SI-traceable calibration of individual instruments from the OCR models, to be followed by laboratories different than the pilot one.
2.	SOW-Req. 30: A routine for periodic re-characterisation and re-calibration shall be defined and established for the OCR models.

3 Introduction

Metrological traceability to the International System of Units [3] is the concept that links all metrological measurements to the SI through a series of calibrations or comparisons. Each step in this traceability chain has a rigorous documented uncertainty analysis. A number of Round-Robin Experiments arranged during the last decades for testing and validation of performance, calibrations and characterisations of Ocean Colour Radiometer (OCR) instruments clearly demonstrated that firm traceability of measurements to the SI units is achievable, and calibration at an National Metrology Institute (NMI) or at an accredited laboratory is the preferred option. The spectral responsivity of a radiometer is usually determined by measuring a known radiation source aligned with specified geometry. Procedures are well established and validated [1], [4]–[8]. Unfortunately, specified and controlled conditions during the calibration in a laboratory may quite differ from varying conditions, which may prevail during later use of the instrument. There can be significant differences between calibration and later field use regarding operating temperature, angular variation of the light field (especially for irradiance sensors), the intensity of the measured radiation, spectral variation of the target, etc. Each of these factors may affect instrument properties when used in the field, and estimation of such uncertainties requires instrument characterisation in addition to the absolute radiometric calibration [2], [9], [10]. This is especially valid even under the most ideal field conditions used for the satellite measurements when the instrument-related corrections/uncertainties are large.

Regular recalibration and complete cal/char of OCRs is needed due to significant drift in responsivity of sensors, possible bias of single instruments, and accounting for environmental factors, which may affect the results. Effective application of cal/char results for calculation of results and related measurement uncertainty is possible if sufficiently detailed definition of the measurand is available including measurement scheme with a number of sensors used, number of repetitions with light and dark signal, measurement sequence and synchronisation information, integration times, etc. The uncertainty also depends on the capability of used radiometers (hard- and software), and about quality of information for additional input quantities (environmental temperature, wind speed, etc.).

A comprehensive characterisation of radiometers and the implementation of correction schemes allows reducing uncertainties in field data. If only a single radiometer is used, then the application of cal/char data is quite straightforward, and cal/char uncertainties contribute to the overall uncertainty budget of the measurement result in the whole amount. For a two radiometer scheme, cal/char contributions to the uncertainty can be rather similar to the single radiometer case, for example with two radiance sensors, which can be used for determination of the normalized water leaving radiance L_{wn}. However, if for the determination of remote-sensing reflectance the system of three radiometers is used then data handling, including uncertainty contributions can be substantially more complicated. In particular, for above-water measurements, often three different radiometers are concurrently used, one measuring the upwelling radiance from the sea, $L_u(\lambda)$, second the downward radiance from the sky, $L_d(\lambda)$ and third, the downward irradiance, $E_d(\lambda)$. Some comments are given below.

The water-leaving reflectance spectra can be calculated from the well-synchronised time series measured with the three-radiometer system. Calculations include the following steps:

1) all measured radiance and irradiance spectra are corrected for the stray light, non-linearity, thermal effects, etc.;
2) spectral response functions of a satellite sensor are used to convolve L_u, L_d and E_d spectra into the satellite spectral bands [11];
3) the water-leaving reflectance $\lfloor \rho_w \rfloor_N$ is calculated as

$$\lfloor \rho_w \rfloor_N = \pi R_{rs}(\lambda) = \pi \frac{L_u(\lambda) - \rho(w_s) L_d(\lambda)}{E_d(\lambda)}, \tag{1}$$

where $R_{rs}(\lambda)$ is the remote sensing reflectance, $L_u(\lambda)$ is the upwelling radiance from the sea, $L_d(\lambda)$ is the downward radiance from the sky, $E_d(\lambda)$ is the downward irradiance and $\rho(w_s)$ is the sea surface reflectance as a function of the wind speed. The spectra of E_d, L_u and L_d are presented in *Figure 3-1.* left as an example of the simultaneous use of three radiometers. In *Figure 3-1* right is remote sensing reflectance calculated from these spectra and convolved to OLCI bands.

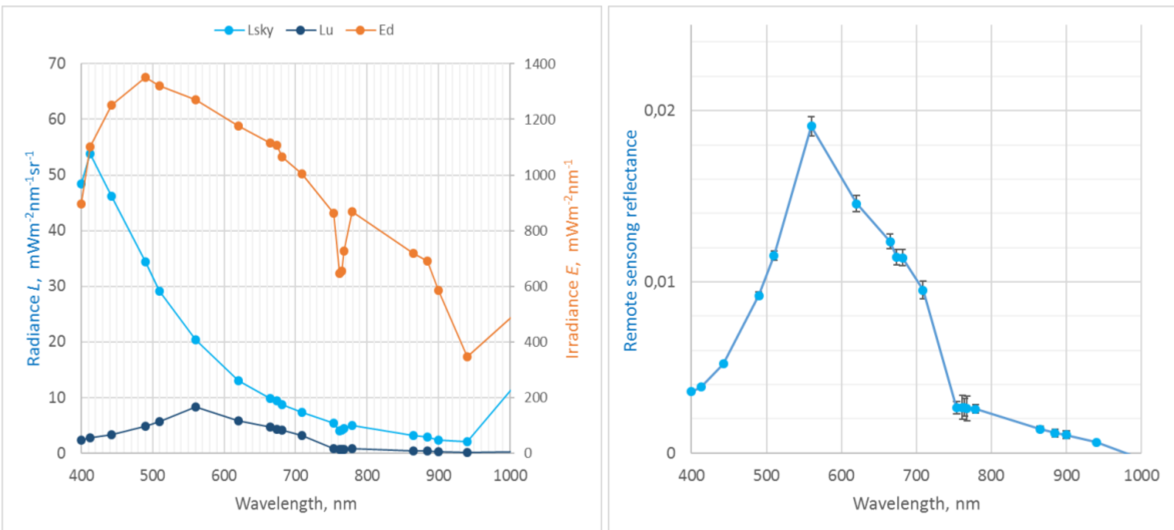

Figure 3-1. Spectra measured with three radiometers (left) for determination of remote sensing reflectance (right) convoluted to OLCI bands. With uncertainty bars, combined expanded uncertainty is shown.

Some environmental conditions affecting radiometers are similar or almost the same (ambient temperature) for all sensors. Some are rather different, like the intensity of radiation, and spatial or spectral distribution, as seen in *Figure 3-1*.

If for the radiometric calibration of the three-radiometer system, the same standard lamp has been used for calibration of all three sensors measuring, respectively, E_d, L_u and L_d, then the contribution of the lamp calibration uncertainty cancels almost fully out. Only contributions from the mechanical alignment of the lamp, plaque and sensors, inadequate baffling, short-time instability of the irradiance standard, and uncertainty of the diffuse reflectance plaque will be relevant. However, this is only valid if the same standard lamp has been used for all sensors in a short space of time (a week or two). This does not mean that absolute calibration of radiometers is not fundamental – without calibration, the comparability of spectra cannot be expected.

In the same way, if we assume identical behaviour for thermal sensitivity of all three sensors the temperature correction will cancel out. Thus, for the three-radiometer system (with all radiometers belonging to the same class), class-based temperature corrections would have no effect on results. This, again, does not mean that in the case of a three-radiometer system, the temperature corrections are always insignificant. If real individual experimental temperature characteristics are used, the thermal correction for a deviation of about 10 °C from the temperature during calibration may be several percent. Here, the differences between the thermal coefficients of different sensors are critical, and due to different thermal loads of the radiometers, temperature differences from calibration points may also be different.

Regarding corrections for non-linearity or stray light, even the same (class-based) characteristics will lead to different corrections due to significant spectral differences. Individual characteristics of radiometers certainly will be preferable. For uncertainty contributions of the three-radiometer system, instead of individual characterisation parameters, the differences between different radiometric sensors will be more relevant.

An example showing possible combined contributions of different uncertainty sources for three-radiometer system of RAMSES and HyperOCR radiometers is in *Figure 3-2*. Here, $\delta x(\text{str})/R$ is relative contribution due to straylight, $\delta x(\text{nlin})/R$ due to nonlinearity and $\delta x(\pm 20\ °\text{C})/R$ are showing relative biases due to temperature differences during calibration and later use. Different thermal effect is due to difference in thermal coefficients (*Figure 6-8*). Possible temperature differences of radiometers during field deployment are not accounted for.

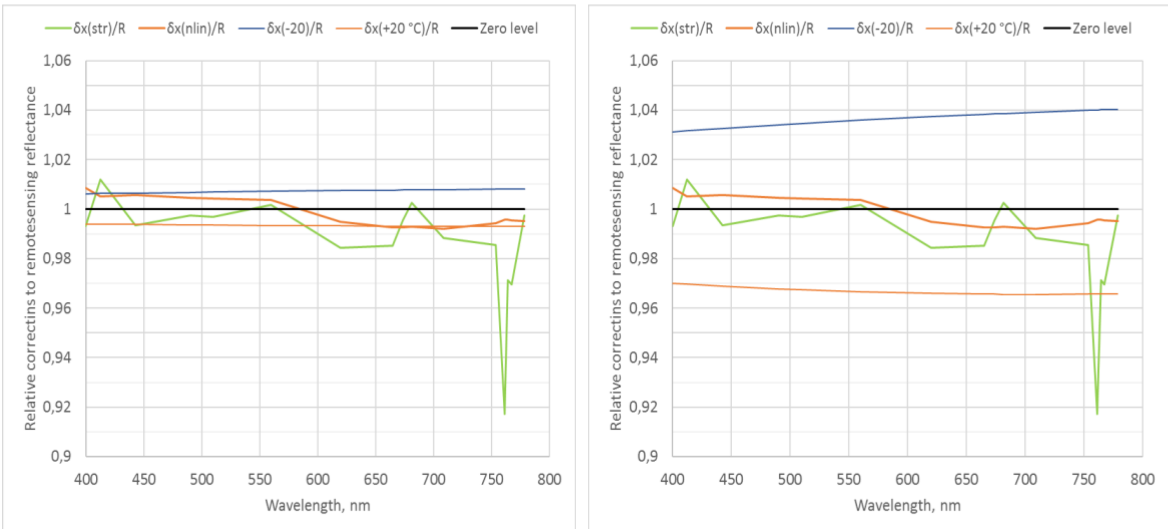

Figure 3-2. Simulation of joint relative effects for the three-radiometer's system due to straylight, nonlinearity and temperature difference during calibration and later use. Left: System with three RAMSES sensors; Right: system with three HyperOCR sensors.

The complete calibration and characterisation scheme for the two OCR classes (TriOS RAMSES and Sea-Bird Scientific HyperOCR) was designed by following the guidelines of the IOCGG protocols [2] and the measurements performed in FRM4SOC Phase-1 [9]. The structure of guidelines for individual characterisation and calibration of hyperspectral OCR needed for the full description and specification of radiometers is presented in Table 3-1 and further discussed in the following sections of this document. Until a better understanding of the class-specific behaviour becomes available, the same cal/char schedule should be applied to radiometers of other types.

The number of OCRs subject to full cal/char during phase-2 was 37, but 5 instruments failed during meausrements, and not all cal/char results were available when preparing the document. Description of radiometers subject to calibration and characterization is given in Section 4. Guidelines for individual calibration of OCR are presented in Section 5. Guidelines for characterisation of FRM OCR instruments is presented in Section 6 following guidlines of the IOCGG protocols [2]. Gaps in cal/char results of FRM OCR are presented in section 7, re-characterisation routine in section 8, and conclusions are presented in section 9.

Table 3-1. Structure of guidelines for the complete char/cal of hyperspectral OCR.

Parameter	**Section**
1. Absolute calibration for radiometric responsivity	5.1
2. Long term stability	5.2
3. Straylight and out of band response	6.1
4. Immersion factor (radiance, irradiance)	6.2
5. Angular response of irradiance sensors in air	6.3
6. Response angle (FOV) of radiance sensors in air	6.4
7. Non-linearity	6.5
8. Accuracy of integration times	6.6
9. Dark signal	6.7
10. Thermal sensitivity	6.8
11. Polarisation sensitivity	6.9
12. Temporal response	6.11
13. Wavelength scale	6.11
14. Signal-to-noise ratio	6.12
15. Pressure effects	6.13

4 Description of radiometers subject to calibration and characterisation

These guidelines are directed to two classes of hyperspectral radiometers: TriOS RAMSES (radiance and irradiance) and the Seabird's HyperOCR (radiance and irradiance) (Table 4-1, *Figure 4-1*). Guidelines are based on complete cal/char of 40 radiometers carried out in the frame of FRM4SOC-2 project.

Table 4-1. Key parameters of the radiometers

Parameter	**Unit**	**RAMSES**		**HyperOCR**	
		irradiance	radiance	irradiance	radiance
weight	kg	0.9		1.1	0.95
length*	mm	295	330	395	355
diameter	mm	48		60(70)	60
supply voltage	V	12**		9…18	
average power consumption	W	0.85		4	
temperature range	°C	+2…+40		-10…+50	
Full-angle field-of-view	°	180	7	180	6***
input aperture diameter	mm	7	15	21	20
wavelength range	nm	350…1000		305…900	
wavelength step	nm	3.3			
spectral bandwidth	nm	9.5			
pixel count	-	256			
integration time	ms	4…8192			
minimum sampling interval	s	1		0.25	
bits per sample	-	16			
responsivity @ 500 nm & 1 ms	$\mu W^{-1} m^2 nm$	0.6	N/A	0.7	N/A
responsivity @ 500 nm & 1 ms	$\mu W^{-1} m^2 nm sr$	N/A	0.1	N/A	0.02
internal shutter	-	no	no	yes	yes
internal temperature sensor	-	no	no	yes	yes

*cable adds 70 mm
**when using the provided cable
*** available also as 23° option

Figure 4-1. Selected radiometer models: 1 - the case, 2 - Seabird's *HyperOCR radiance sensor, 3 - HyperOCR irradiance sensor, 4 - TriOS RAMSES radiance sensor, 5 - RAMSES irradiance sensor, 6 - HyperOCR connection harness, 7 - RAMSES connection harness, 8 - alignment jig, 9 - bubble level.*

The radiometers contain a Zeiss MMS1 module spectrometer, proprietary front-end electronics and optical input elements in the watertight housing. The housing has cylindrical symmetry, with the optical input and signal connector at the opposite ends of the cylinder. The housing is fabricated from stainless steel (RAMSES) or plastic (HyperOCR). The optical axis is expected to coincide with the centre of the cylinder. The wavelength scale and some other parameters are defined in the calibration files provided by the manufacturer.

5 Absolute calibration for radiometric responsivity

5.1 Calibration for radiometric responsivity

Requirement (D-2): IR1

Scope: individual

Type: required

Calibration for the radiometric responsivity is the most basic characterisation measurement of an OCR, establishing the link between the radiometer's output and the SI units. A detailed description of the calibration methods for the irradiance and radiance responsivity is given in p.7 of the D-12.

5.2 The re-calibration schedule

There are several (natural) reasons for the decay of the radiometric responsivity: e.g. ageing of the input optics, collimators/gratings, the sensor and even some components of the front-end electronics. Contamination or heavy damage of the fore-optics can cause responsivity changes of several per cent. Consequently, careful handling, safe deployment and protection (against the bio-fouling) of the instruments should be ensured. The factory-provided cleaning procedures shall be followed for both field and laboratory deployments to get coherent results (while avoiding unnecessary cleaning). Post-deployment calibration of the sensors is a best practice to quantify the responsivity change during the field campaign. The pre-deployment calibration shall always be performed with the clean input optics of the radiometer.

In paragraph 5.3 of the D-7, the calibration history of seven hyperspectral radiometers is presented, calibrated at the optical lab of TO from 2016 to 2022. During this time, different standard FEL lamps have been used with traceability to different NMI-s (MIKES, NPL, TU). At the optical lab of TO, several standard FEL lamps are ready for use and can simultaneously be operated; between calibrations these lamps are regularly compared by using the filter radiometer with silicon trap detector serving as reference for stability of lamps. A more detailed calibration history of five RAMSES and two HyperOCR sensors is shown in D-7. The manufacturing date and type of sensors with calibration history are given in Table 5-1.

Table 5-1. Manufacturing date and type of sensors with calibration history.

Name	Type	Serial number	Manufacturing Date	Mean drift in year
TriOS RAMSES	irradiance	SAM 8329	2010	-0.8 %
TriOS RAMSES	irradiance	SAM 8598	2018	-2.3 %
TriOS RAMSES	radiance	SAM 8166	2004	-1.2 %
TriOS RAMSES	Radiance	SAM 81B0	2006	-1.0 %
TriOS RAMSES	radiance	SAM 8595	2018	-1.1 %
HyperOCR	radiance	SAT 0222	2013	-1.6 %
HyperOCR	irradiance	SAT 0258	2013	-1.1 %

As seen from the data in Table 5-1, the average drift of characterised radiometers is quite similar and close to 1 % per year. Thus, the requirement to recalibrate the radiometers at least once a year is well justified. It is restated that spectral radiometric responsivity should be ideally determined before and after each major field deployment.

6 Description of characterisation methods

6.1 Stray light characterisation

Requirement (D-2): IR2

Scope: individual

Type: recommended

6.1.1 Guidelines for characterisation

Under the term "stray light", we understand the deviating from the ideal of both the in-band (IB) and out-of-band (OOB) response of the OCR, as they are characterised similarly and will have a similar influence on the measurement results. The stray light correction, when used, has to be applied to both the cal/char and the field measurements. Otherwise, systematic errors might be introduced. A description of stray light characterisation procedures is given in D-12. The stray light behaviour is represented in the $n \times m$ matrix [(1)] form where n denotes the number of pixels of the OCR and m the number of excitation wavelengths (graphical representation in *Figure 6-1*). Although the stray light of the proposed OCR types has strong class-specific behaviour, all specimens show specific individual artefacts.

A detailed description of the methods for stray light characterisation is given in p.8.1 of the D-12.

6.1.2 The re-characterisation schedule.

The stray light behaviour is mainly related to the underlying spectrometer of the OCR: to the slits, collimators, gratings, filter transmittances and internal reflections. In the case of compact spectrometer modules, these characteristics are well under control and stable. In the case of open-air modules, contamination and degradation of the optical components might significantly contribute to the stray light behaviour, and re-characterisation after every 3-5 years is recommended. As shown in [12], [13], the stray light behaviour depends on the illumination conditions. Thus, the re-characterisation is recommended whenever the spectrometer module, the sensor or the fore optics are re-aligned or changed. The stray light matrix for RAMSES sensor is shown in *Figure 6-1*.

[(1)] Straylight matrix is a $n \times n$ matrix where n is a number of pixels. Not all pixels are accessible for measurement. Parts of matrix which cannot be determined experimentally are filled by hand in order to use matrix operators needed for calculations.

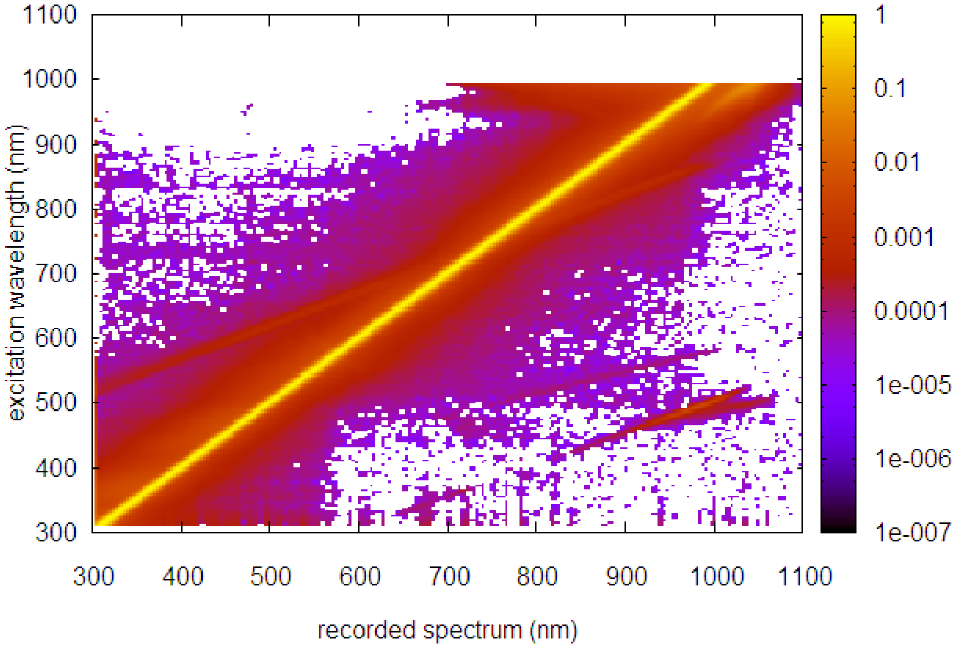

Figure 6-1. Stray light matrix of a RAMSES sensor. Diagonal values of the SLM are narmalised to 1

6.2 Immersion factor (irradiance, radiance)

Scope: required for under-water measurements

Type: individual (irradiance), class-specific (radiance)

6.2.1 Guidelines for characterisation

A detailed description of the methods for characterisation of immersion factor is given in p.8.2 and 8.3 of the D-12.

6.2.2 The re-characterisation schedule

Re-characterisation of irradiance sensors is needed whenever the fore optics is changed or re-aligned.

6.3 Angular response of irradiance sensors in air

Requirement (D-2): IR3

Scope: individual

Type required

6.3.1 Guidelines for characterisation

The angular response (namely, its deviation from the cosine law) is determined by the construction of the irradiance entrance optics and shows strong individual character. This is one of the basic contributors to the measurement uncertainty and has to be quantified for each irradiance sensor before commissioning. Moreover, characterisation set-up is not standardized, and discrepancies between different laboratories and procedures are possible. Slight deviations from the cylindrical symmetry in the case of some OCR specimens introduce systematic alignment errors because of the different parallax in the field and lab illumination geometries. Further systematic errors are related to the tilt of the diffuser with respect to the cylindrical axis, yielding the need for measurements in several scanning planes. The proposed characterisation method is described in D12. Examples of the angular responses are shown in *Figure 6-2*.

6.3.2 Re-characterisation schedule

Re-characterisation is needed after replacement/repair of the fore optics or when the OCR is re-assembled in the workshop because the angular response is very sensitive even to the smallest adjustments of the optical elements and shadow rings [14], [15]. As very little is known about the class-specific temporal changes, re-characterisation every 3-5 years is recommended when applicable to contribute to the common knowledge.

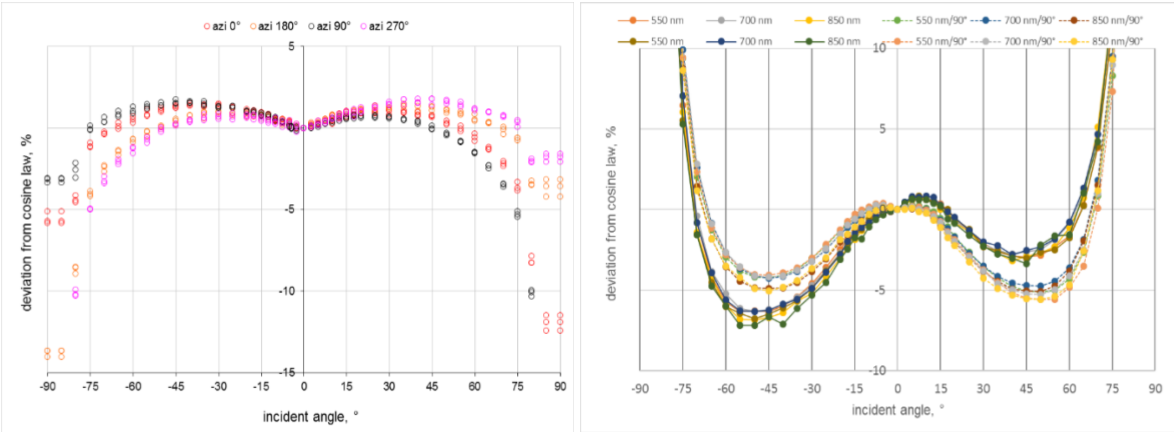

Figure 6-2. Angular response of HyperOCR (left) and RAMSES (right) irradiance sensors.

As evident in *Figure 6-2*, the angular response of irradiance sensors is often asymmetrical. Therefore, in order to guarantee reproducibility of characterisation results of angular measurements, the sensor's azimuth angle shall be clearly defined and specified in the characterisation report.

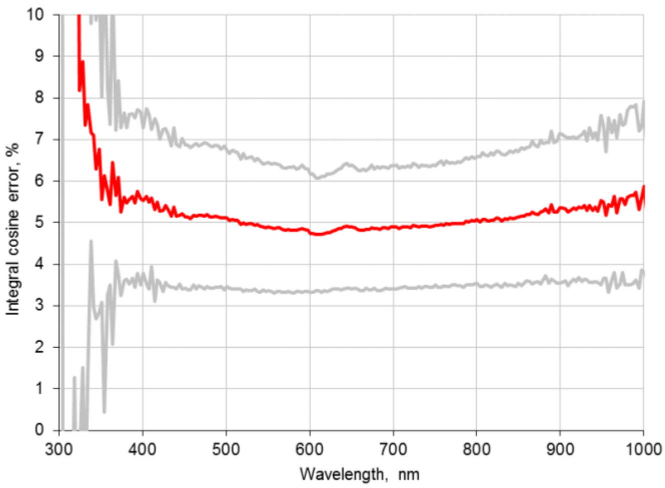

Figure 6-3. Integral cosine error with expanded uncertainty bars of a RAMSES irradiance sensor.

The integral error of the cosine collector of the RAMSES sensor together with the bars indicating limits of expanded uncertainty, is shown in *Figure 6-3*. The cosine response error of RAMSES sensors is often significantly larger than the cosine response error of HyperOCR sensors, with much larger variability between individual sensors.

A detailed description of the methods for characterising the angular response is given in p.8.4 of the D-12.

6.4 Angular response (FOV) of radiance sensors in air

Requirement (D-2): IR3

Scope: individual

Type: recommended

6.4.1 Guidelines for characterisation

The FOV of the radiance sensors of the common OCR types show expected (according to the specification) behaviour. Slight deviations of the FOVs and differences between the symmetry axes of the FOV and the OCR's cylindrical body are within ±0.5° and are expected to have a negligible contribution to the remote sensing products. An example of the FOV is shown in *Figure 6-4*. Relative responsibility is normalised to one for the zero incident angle.

6.4.2 Re-characterisation schedule.

The re-characterisation is recommended after the change of the fore optics or re-assembly of the OCR in the workshop.

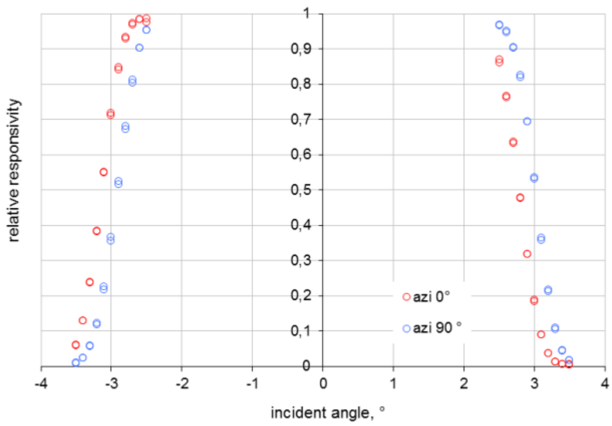

Figure 6-4. FOV of above-water HyperOCR radiance sensors.

A detailed description of the methods for characterisation of the angular response (FOV) is given in p.8.5 of the D-12.

6.5 Non-linearity of response

Requirement (D-2): IR4

Scope: individual

Type: recommended

6.5.1 Guidelines for characterisation

Measurements of non-linearity correction coefficients can be based solely on measurements of radiant exposure from a stable light source with different integration times. Radiant exposure is the radiant energy received by a surface per unit area or equivalently the irradiance of a surface, integrated over time of illumination. To determine the radiometric non-linearity, a stable source (e.g. the calibration source) must be measured using at least two different integration times. This can be done easily during the radiometric calibration. Data averaging and dark measurements must be applied accordingly. The corrected spectrum $S_{1,2}(n)$ is calculated as

$$S_{1,2}(n) = \left[1 - \left(\frac{S_2(n)}{S_1(n)} - 1\right)\left(\frac{1}{t_2/t_1 - 1}\right)\right] S_1(n), \tag{2}$$

where $S_1(n)$ and $S_2(n)$ are the raw signals of pixels $n \in (0,255)$ measured with integration times of t_1 and t_2, respectively, after scaling up to the largest used integration time. The corrected signal $S_{1,2}(n)$ is shown to be independent of the selection of t_1, t_2, but the smaller the integration time t_i, the closer the signal S_i to the corrected signal. Thus, $S_{1,2}(n)$ is asymptotically approaching the integration time limit value of 0 ms. The standard deviation of $S_{1,2}(n)$ is substantially determined by the signal with the shortest integration time.

A detailed description of the methods for characterisation of the non-linearity of response is given in p.8.6 of the D-12. For the setup, pre-heating and uncertainty, consider the guidelines in D-12, section 8.1 and 8.2.

6.5.2 Re-characterisation schedule.

It is recommended to perform the non-linearity characterisation together with the radiometric calibration. It shall be performed after the change of the fore optics or re-assembly of the OCR in the workshop.

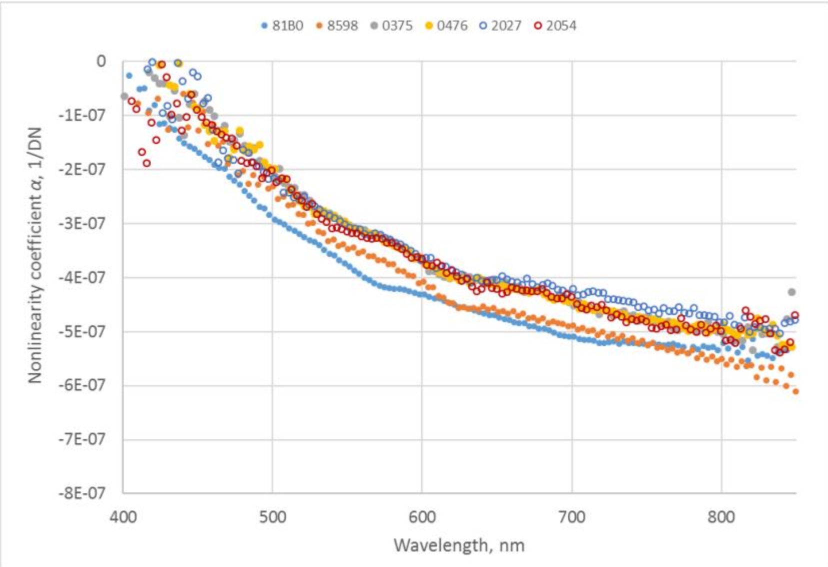

Figure 6-5. Averaged non-linearity coefficient α of two RAMSES and four HyperOCR sensors.

In *Figure 6-5*, averaged non-linearity coefficient α for six radiometers is presented. RAMSES sensors are shown with two lower curves, HyperOCR sensors with a group of upper curves. For both instrument models, the class-based approach of correcting for the non-linearity effect seems acceptable.

The non-linearity correction for a remote sensing reflectance means that altogether six raw spectra have to be corrected - two for each radiometer because non-linearity correction needs to be also applied for the standard source spectrum during the responsivity calibration.

6.6 Accuracy of integration times

Scope: individual

Type: individual characterisation recommended

6.6.1 Guidelines for characterisation

The integration times of the characterised OCR classes expand from a few milliseconds up to a few seconds. The accuracy of the integration time is difficult to measure directly without disassembling the instrument or building sophisticated testing equipment. However, the error of the integration time will be directly carried over to the measurement result (unless the class-specific errors cancel out if setups with two or three radiometers are used).

During the FRM4SOC phase-2 laboratory characterisations, from all non-linearity results obtained for more than 40 radiometers, a clear deviation from the set values of the integration time was found in the case of the shortest (4 ms) integration time. The measurement method is described in D12. An example for a HyperOCR radiance sensor is in

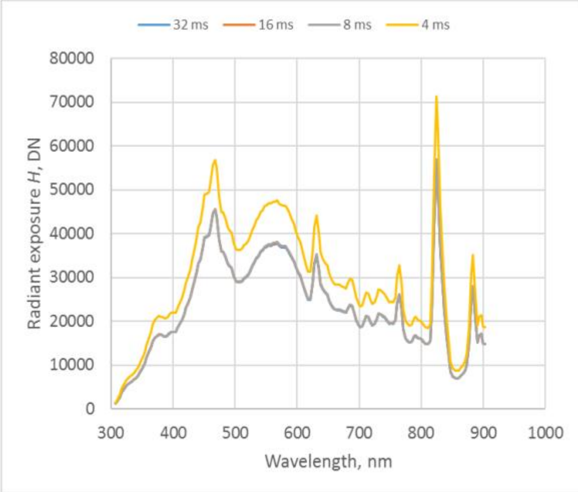

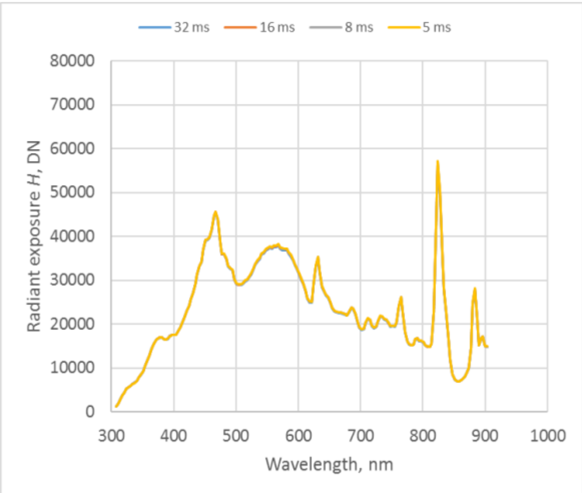

Figure 6-6. The Xe-lamp spectra are measured by using four different integration times and normalised to the same radiant exposure. On the left panel, the spectrum measured with the set value of 4 ms is significantly deviating from the other three spectra (overlapping on the figure). After transforming the shortest integration time from the initial 4 ms to the expected actual value of 5 ms, good agreement is evident on the right panel. In the case of the RAMSES instruments, the actual integration time was around 4.05 ms instead of 4 ms. Minor errors at longer integration times can not be easily detected, but they contribute to the estimate of radiometric non-linearity instead. Likely reason for the spread of individual non-linearity characteristics is due to small variability of realized integration times (for RAMSES sensors, relative changes within 1±0.001 are evident).

6.6.1. Re-characterisation schedule.

The re-characterisation is not necessary unless the electronic parts of the OCR are repaired in the workshop.

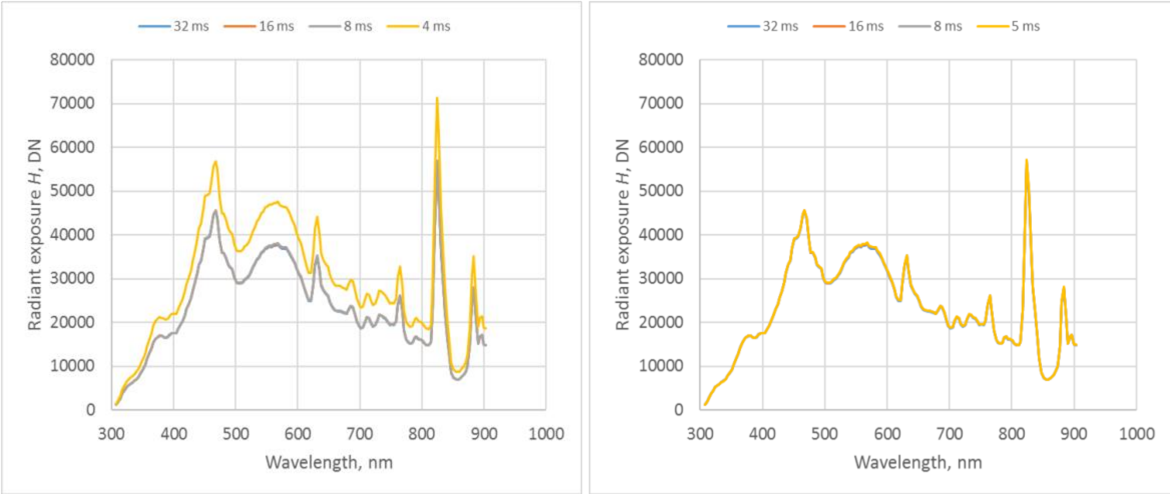

Figure 6-6. Xe-lamp spectra measured by using four integration times and normalised to the same radiant exposure. Left: for the value set to 4 ms large bias is evident; right: after applying the actual value of 5 ms normal agreement is achieved.

Integration time errors shall be determined at least for the region of shorter integration times that will be routinely used in either field or calibration measurements. Different errors like mechanical shutter speed limitation, timing offsets, or any factors related to charge handling from the detector array elements are more likely for this region than with longer integration times.

A detailed description of the methods for characterisation of the accuracy of integration times is given in p.9 of the D-12. However, the proposed simplified method is suitable to detect deviations at the shortest integration times.

6.7 Dark signal

Requirement (D-2): IR7

Scope: individual

Type: required

6.7.1 Guidelines for characterisation

The standard deviation of the dark signal shows the performance of the front-end electronics, while the absolute level can be used as a proxy for the instrument's internal temperature. Both the average bias and the standard deviation depend on the integration time. For the dark characterisation, the optical input of the OCR has to be covered unless the internal mechanical shutter is used. The background measurement during certain cal/char measurements might not be valid for dark signal characterisation. The handling of the dark signal is described in the corresponding chapters of D12.

6.7.2 Re-characterisation schedule

A periodic check of the dark signal is recommended during the instrument exploitation, as it can help reveal some electronic and power issues. The artefacts suggesting the need for repair/maintenance are oscillations, temporal drifts not explained by temperature change and sudden jumps in bias level (see *Figure 6-7*).

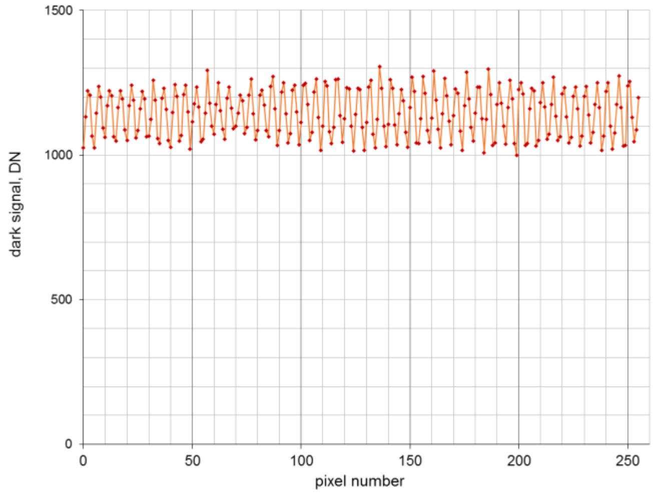

Figure 6-7. Oscillations of the dark signal implying the need for repair.

A detailed description of the methods for characterising the dark signal is given in p.8.7 of the D-12.

6.8 Thermal response

Requirement (D-2): IR5

Scope: individual

Type: required

6.8.1 Guidelines for characterisation

The thermal response is amongst the most time- and effort-consuming characterisation parameters of the OCR, but the contribution to the field measurement results can exceed 10% under certain conditions when not corrected. As in general, the thermal response of the OCR's output signal consists of the thermal response of the linear optical sensor (which has strong class-specific behaviour) and the thermal change of the electronic bias (rather specific to each OCR specimen). Due to the underlying physics, both the dark and light signal of the uncooled photoelectric sensor depend on temperature. On the other hand, electronic bias can have an arbitrary temperature coefficient with changing sign and magnitude. Bi-stability of the electronic biases is observed during the FRM4SOCII lab characterisation measurements. The thermal response coefficients depend on the integration time. The strongest thermal response of the dark signal is obtained with the longest integration time and can be used as a proxy for the instrument's internal temperature. This proxy can, in certain cases, be more reliable than the built-in temperature sensor. Most of the thermal contributions depend on the temperature differences during the cal/char and field measurements. Good knowledge of the instrument's internal temperature is vital when correcting for the ambient temperature during the field measurements. Despite that, it is well known and confirmed during the FRM4SOC lab measurements that the PTFE material, often used in diffusers, has phase change at +19 °C, contributing to the measurement error [15], [16]. This error is more closely related rather with the external (case) temperature of the OCR. The laboratory characterisation measurements show that thermal relaxation inside the radiometer can take more than an hour and depends on the acquisition mode (via self-heating). Moreover, even the arbitrary slow change (~1 °C/min) of ambient temperature can introduce hysteresis in the radiometer's output signal up to 6% depending on the direction of the temperature change. Thermal corrections might partly cancel out with certain measurement setups with two-three radiometers due to the class-specific behaviour. However, variability in instrument's parameters within a given class up to ±10% (*Figure 6-8*) will limit the uncertainty of the OC products if not corrected for. In other cases, for example when validating *E*d, the thermal responsivity of the individual OCR will fully affect the measurement result.

6.8.2 Re-characterisation schedule

The re-characterisation is not necessary unless the electronic parts of the OCR were repaired or the linear sensor or fore optics were replaced in the workshop. Re-characterisation after 3-5 years and using different laboratories is recommended in order to collect more experience and to foster the development of the characterisation methods.

Thermal coefficients of two RAMSES and four HyperOCR sensors are presented in Figure *6-8*. For determination of the thermal coefficients, the radiometer was immersed into a cylindrical thermally controlled water tank, equipped with an optical grade fused silica window. The temperature set points were selected in the range from +5 °C to +40 °C to cover the expected temperature range evenly as in use. Three integration times have been used at each set point to account for the non-linearity effect.

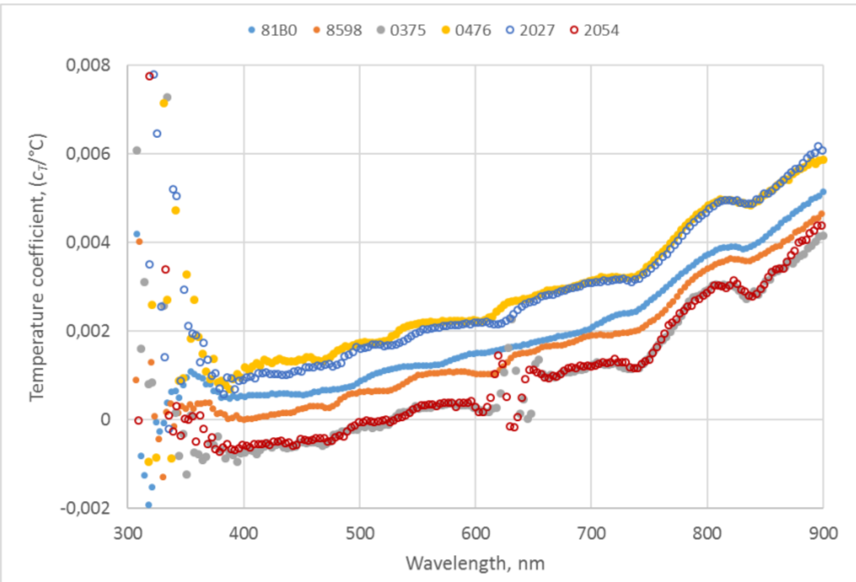

Figure 6-8. Thermal coefficients of two RAMSES and four HyperOCR sensors after correction for non-linearity.

All thermal coefficients presented in *Figure 6-8* are rather similar. Two middle curves belong to the RAMSES radiance and irradiance sensor. Two lower curves belong to the HyperOCR radiance sensor, and two upper curves to the HyperOCR irradiance sensors. For all groups, a class-based approach to correct for temperature difference during calibration and later use is possible, but only in the case of applications where a single radiometer is used.

Seabird's Sensor System Group [17] provides guidance on how to apply thermal responsivity correction to an instrument's optical sensor data. Calculated thermal characteristics for an irradiance and a radiance sensor using this algorithm are shown in *Figure 6-9* with bold dashed lines. Characterisation data for three irradiance and four radiance sensors are given with continuous lines. The averaged value of characterisation data is shown with the red dotted line. Although averaged and calculated (specification) values are rather close, differences between individual radiometers are significant, and uncertainty due to the thermal responsivity of some radiometers without characterisation could be easily underestimated.

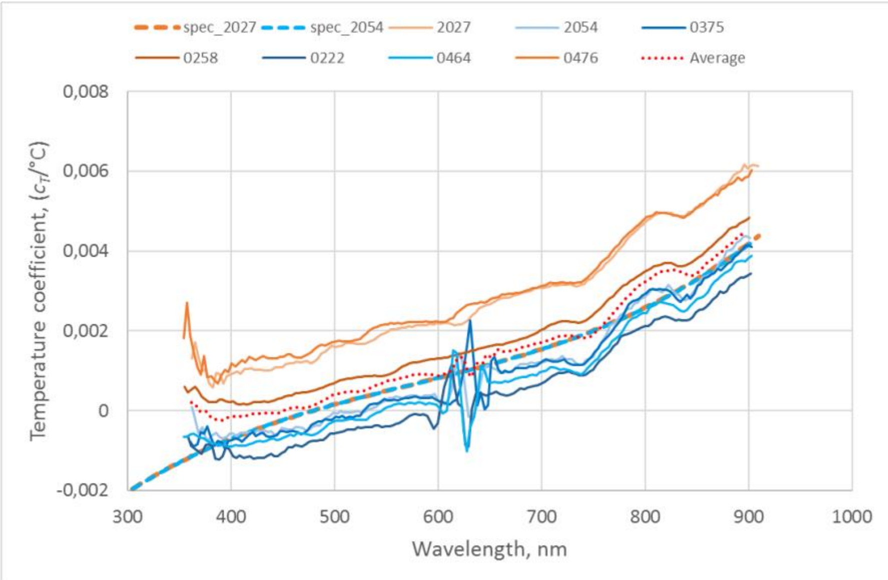

Figure 6-9. Thermal coefficients of seven HyperOCR sensors and thermal responsivity data for two sensors calculated according to the guidance of the Seabird's *Sensor System Group.*

A detailed description of the methods for characterisation of the thermal response is given in p.8.8 of the D-12.

6.9 Polarisation sensitivity

Requirement (D-2): IR6

Scope: class-specific

Type: recommended

6.9.1 Guidelines for characterisation

Light from the sea has a degree of polarisation varying with water constituents and the atmospheric aerosols with impact are more pronounced in above-water radiometry. Both the clear sky radiance and the light reflected from the water surface and from the clouds are partially polarised. Therefore, the polarisation sensitivity of radiometers due to individual optical components (e.g., optical windows, lenses, dispersive elements) becomes a source of uncertainty in measurements. Unless special measures are taken during the field measurements, the polarisation sensitivity has to be fully included in the field uncertainty budget.

Examples of the polarisation sensitivity of selected OCRs as a function of angle and wavelength is presented in *Figure 6-10*.

6.9.2 Re-characterisation schedule

The re-characterisation is not necessary unless the forensics or spectrometer module of the OCR were repaired or replaced in the workshop.

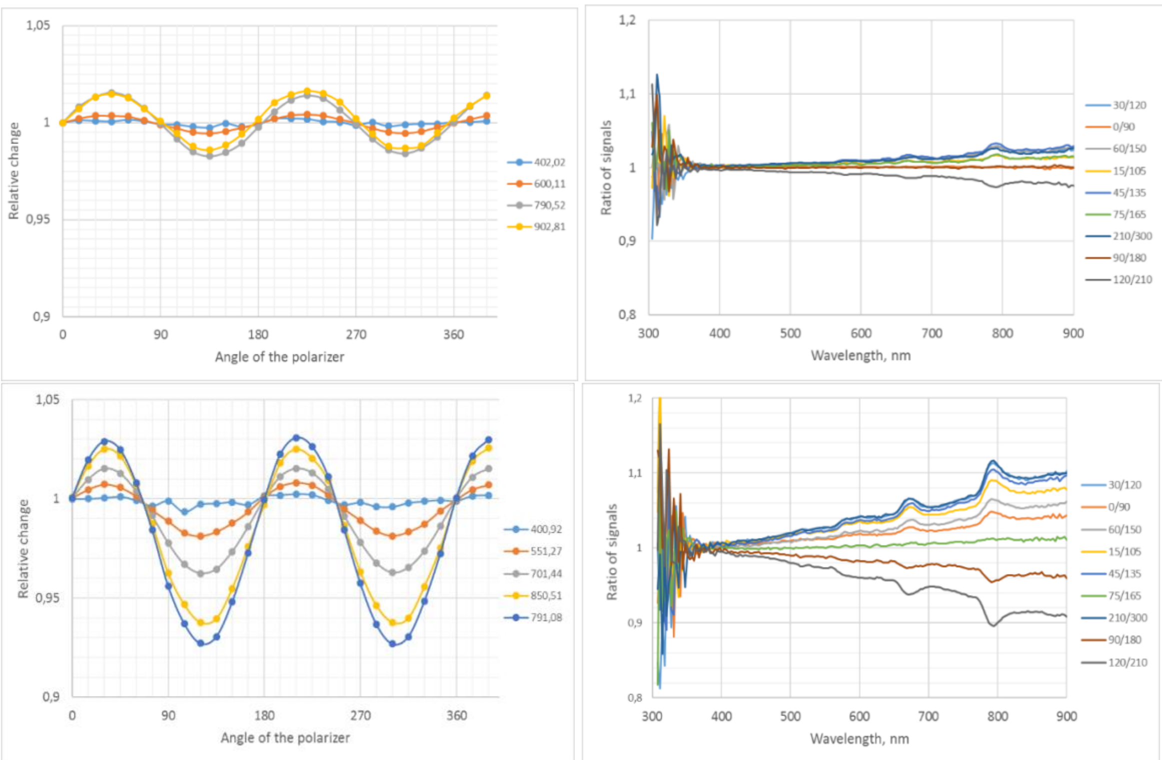

Figure 6-10. Relative polarisation effect as a function of angle and wavelength. RAMSES radiance sensor (upper part) and HyperOCR radiance sensor (lower part).

A detailed description of the methods for characterisation of the polarisation sensitivity is given in p.8.9 of the D-12.

6.10 Temporal response

Requirement (D-2): IR8

Scope: TBD

Type: TBD

6.10.1 Guidelines for characterisation

TBD

6.10.2 Re-characterisation schedule

TBD.

6.11 Accuracy of wavelength scale

Requirement (D-2): IR9

Scope: class-specific

Type: recommended

6.11.1 Guidelines for characterisation

The accuracy of the wavelength scale of the characterised OCR specimen does not show significant deviation from the factory specification over the full temperature range. The wide bandwidth (~10 nm) of the RAMSES and HyperOCR instruments does not allow to model thin features of the remote sensing spectra, and the possible shift of the wavelength scale of the individual OCRs (<0.5 nm) will not contribute much to the final uncertainty budget. However, when using radiometers with higher resolution (~1 nm) and investigating fine features of the spectra (e.g. slopes of the absorption/reflection bands), contribution to the uncertainty budget has to be determined according to the application, and individual characterisation of the OCR for the wavelength scale accuracy might be necessary. Characterisation setup and method are described in D12. Agreement of the wavelength scale at selected wavelengths/temperatures with Kr-lamp reference values is shown in Table 6-1.

6.11.2 Re-characterisation schedule

Table 6-1. Difference of measured wavelengths from Kr-lamp reference values.

Name	Temperature	λmeas	Δλ1	λmeas	Δλ 2	λmeas	Δλ 3
RAMSES_L	5 °C	557	0.12	759.9	0.05	811.32	0.19
RAMSES_L	20 °C	556.9	0.02	759.95	0.1	811.3	0.17
RAMSES_L	40 °C	556.82	-0.06	759.82	-0.03	811.2	0.07
RAMSES_E	5 °C	556.75	-0.13	759.77	-0.08	811.05	-0.08
RAMSES_E	20 °C	556.6	-0.28	759.65	-0.2	811	-0.13
RAMSES_E	40 °C	556.7	-0.18	759.65	-0.2	810.87	-0.26
HyperOCR_L	5 °C	556.88	0	759.63	-0.22	810.9	-0.23
HyperOCR_L	20 °C	556.84	-0.04	759.72	-0.13	810.8	-0.33
HyperOCR_L	30 °C	556.95	0.07	759.82	-0.03	811.05	-0.08
HyperOCR_L	40 °C	556.72	-0.16	759.6	-0.25	810.75	-0.38
HyperOCR_E	5 °C	556.75	-0.13	759.82	-0.03	811.04	-0.09
HyperOCR_E	20 °C	556.62	-0.26	759.75	-0.1	810.95	-0.18
HyperOCR_E	40 °C	556.55	-0.33	759.64	-0.21	810.85	-0.28

A detailed description of the methods for characterisation of the accuracy of the wavelength scale is given in p.8.11 of the D-12.

6.12 Signal-to-noise ratio

Scope: individual

Type: recommended

6.12.1 Guidelines for characterisation

As in the case of dark signal, signal-to-noise ratio (SNR) can be used not only to evaluate the uncertainty of lab and field measurements but also for detection of the instrument malfunction. The SNR, when defined according to D-12, depends on the temperature and signal level but weakly on the integration time; one should distinguish the light and dark SNR. SNR is typically determined by the OCR class, but individual deviations are inevitable. As the field conditions are variable by definition, determination of the SNR directly from the field measurements is difficult, and the laboratory-measured SNR has to be kept in mind as the lowest possible standard deviation at given temperature, illumination level and integration time. The individual characterisation is recommended due to the simplicity of the measurements, i.e. specialised laboratory equipment is not needed. The signal-to-noise ratio and SNR as a function of raw signal level is shown in *Figure 6-11*.

6.12.2 Re-characterisation schedule

Yearly re-characterisation as the side product of the radiometric calibration. Additional check during/after major field campaigns in order to detect instrument malfunctioning.

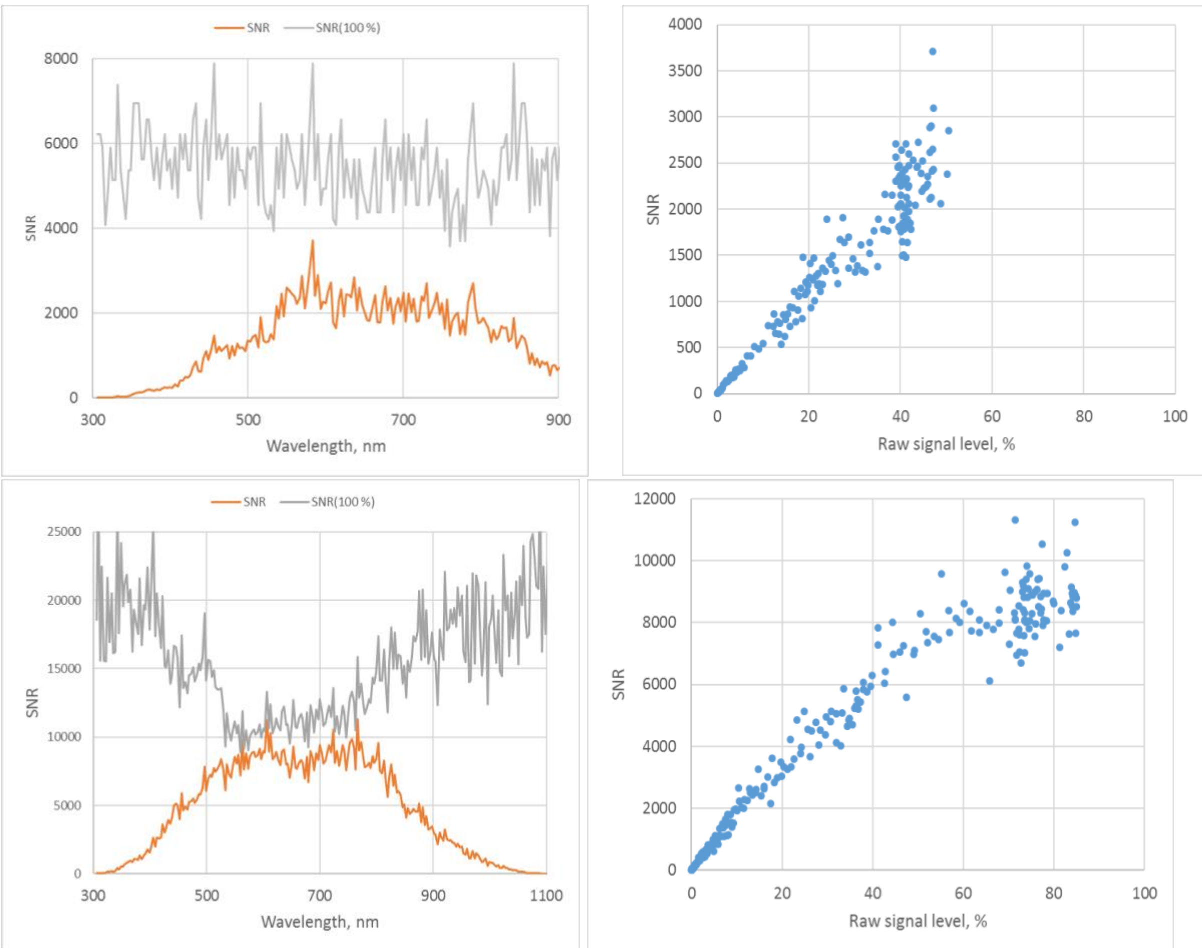

Figure 6-11. Signal-to-noise ratio (left) and SNR as a function of raw signal (right). HyperOCR radiometer (upper part) and RAMSES (lower part).

A detailed description of the methods for characterisation of the signal-to-noise ratio is given in p.8.12 of the D-12.

6.13 Pressure effects

Scope: TBD

Type: TBD

6.13.1 Guidelines for characterisation

Characterisation in progress.

6.13.2 Re-characterisation schedule

TBD

7 Gaps in characterisation guidelines

Table 7-1. List of parameters to be updated in the following versions of the document (D-8).

Parameter	Plans for characterisation
Accuracy of integration times	Planned during the project at UT
Temporal response	Planned during the project at UT
Pressure effects	Planned during the project at UT
Immersion coefficients	Preformed at JRC, analysis is going on.

8 Calibration and re-characterisation routine

The calibration re-characterisation routine is presented in Table 8-1.

Table 8-1. Guidelines for individual OCR calibration/characterisation and the re-characterisation schedule.

Parameter	Scope	Before initial use	Re-cal/char	D-2 requirement
1. Absolute calibration for radiometric responsivity	individual	required	1 year	IR1
2. Long term stability	individual	required	after every calibration	IR1
3. Stray light and out of band response	individual	required	3 – 5 years	IR2
4. Immersion factor (irradiance)	individual	required for under-water	after fore-optics modification	-
4b.Immersion factor (radiance)	class-specific	-	after fore-optics modification	-
5. Angular response of irradiance sensors in air	individual	required	after fore-optics modification	IR3
6. Response angle (FOV) of radiance sensors in air	individual	required	after fore-optics modification	-
7. Non-linearity	individual	required	after repairs	IR4
8. Accuracy of integration times	individual	required	after repairs	IR4
9. Dark signal	individual	required	1 year	IR7
10. Thermal responsivity	individual	required	after repairs	IR5
11. Polarisation sensitivity	class-specific	-	-	IR6
12. Temporal response	TBD	TBD	TBD	IR8
13. Wavelength scale	class-specific	-	-	IR9
14. Signal-to-noise ratio	individual	required	1 year	-
15. Pressure effects	TBD	TBD	TBD	-

9 Conclusions

TR D-8, Guidelines for individual OCR full characterisation and calibration is intended as methodical aid for the FRM measurement scientist/teams, for secondary labs active in the OC cal/char, and for beginning OC calibration laboratories. Guidelines for individual OCR calibration/characterisation and the re-characterisation schedule are summarised in Table 8-1. The structure of the document and list of parameters is the same/similar as in documents D-2, D-7, and D-12. The most important part of cal/char activities is the absolute radiometric calibration of spectral responsivity required individually and regularly for all OCR-s at least once a year. Mostly required characterisations are the angular response of irradiance sensors in air, immersion factor of irradiance sensors in water, thermal sensitivity and dark signal. Nevertheless, before the field use of OCR-s all other characterisations listed in Table 8-1 are also highly recommended.

Class specific characterisation of OCRs and respective instrument classes have limited applicability as individual characteristics of many parameters determined during the FRM4SOC Phase 2 had rather large spread. Initially, radiometers from a given manufacturer were assumed to form a single class as the parameters are linked to the opto-electronical design within the production line. Based on the characterisation results, four instrument classes have been considered: radiometers from each manufacturer were subdivided into two classes according to the input optics (radiance vs. irradiance). Class-specific characterization results are calculated as averages of the individual parameters from the instruments belonging to that particular class. Class-specific expanded uncertainty shall cover about 95 % of all determined individual parameters. The class-based characterization data is continuously updated as the new characterization results become available. The class-based data will be used in the cases were the individual data is not available. Both the individual and class-based characterization data are stored into the database and used by the Community Processor.

The calibration procedures of the absolute spectral responsivity are well established and validated. However, unfortunately, there can be significant differences between the calibration and later field use, as regards operating temperature, angular variation of the light field (especially for irradiance sensors), the intensity of the measured radiation, and spectral variation of the target etc. Each of these factors may interact with instrument imperfections when used in the field, and estimation of such uncertainties requires instrument characterisation in addition to the absolute radiometric calibration [2], [9], [10]. Furthermore, most calibrations and characterisations are performed in strictly controlled stable conditions, but field measurements are often in variable or strongly varying conditions. Regarding the results of dynamic characterisations described in D-7, some dynamic characterisations would be indispensable to achieve firm SI traceability.

An important outcome of dynamic tests is the large hysteresis of optical response and its strong dependence on the particular location of the temperature sensor used for the data presentation. Large hysteresis can easily happen when radiometers without an internal temperature are used, and it may significantly contribute to errors affecting results.

Thanks to dynamic temperature scanning, the anomalous behaviour of cosine collectors of HyperOCR irradiance sensors has been detected.

Specifying the sensor's temperature is a critical issue, especially for sensors without an internal temperature sensor installed in the close vicinity of the optical sensor. To some extent, using the dark signal to determine the temperature of the optical sensor may be helpful. However, calibration of internal sensors or validation of calculated temperature values still is problematic. The internal temperature sensor cannot be taken out of the radiometer for calibration, even if it is present. There is no effective reference for validation of calculated internal temperatures, in the other case for instruments not equipped with internal sensors.

10 References

[1] J. L. Mueller *et al.*, "Ocean Optics Protocols For Satellite Ocean Color Sensor Validation, Revision 4. Volume III: Radiometric Measurements and Data Analysis Protocols.," 2003, doi: http://dx.doi.org/10.25607/OBP-62.

[2] "IOCCG Protocol Series (2019). Protocols for Satellite Ocean Colour Data Validation: In Situ Optical Radiometry. Zibordi, G., Voss, K. J., Johnson, B. C. and Mueller, J. L. IOCCG Ocean Optics and Biogeochemistry Protocols for Satellite Ocean Colour Sensor Validation, Volume 3.0," IOCCG, Dartmouth, NS, Canada, 2019. doi: http://dx.doi.org/10.25607/OBP-691.

[3] "JCGM 200:2008: International Vocabulary of Metrology - Basic and General Concepts and Associated Terms (VIM)." BIPM, Aug. 2011.

[4] S. B. Hooker *et al.*, "The Seventh SeaWiFS Intercalibration Round-Robin Experiment (SIRREX-7), TM-2003-206892, vol. 17, NASA Goddard Space Flight Center, Greenbelt," Feb. 2002, Accessed: Feb. 08, 2017. [Online]. Available: http://ntrs.nasa.gov/search.jsp?R=20020045342

[5] L. Ylianttila, R. Visuri, L. Huurto, and K. Jokela, "Evaluation of a Single-monochromator Diode Array Spectroradiometer for Sunbed UV-radiation Measurements¶," *Photochem. Photobiol.*, vol. 81, no. 2, pp. 333–341, 2005, doi: 10.1111/j.1751-1097.2005.tb00192.x.

[6] G. Seckmeyer, "Instruments to Measure Solar Ultraviolet Radiation Part 4: Array Spectroradiometers (lead author: G. Seckmeyer) (WMO/TD No. 1538). 44 pp. November 2010." WMO, 2010.

[7] C. Johnson, H. Yoon, J. P. Rice, and A. C. Parr, "Chapter 1.2 - Principles of Optical Radiometry and Measurement Uncertainty," in *Experimental Methods in the Physical Sciences*, vol. 47, G. Zibordi, C. J. Donlon, and A. C. Parr, Eds. Academic Press, 2014, pp. 13–67. doi: 10.1016/B978-0-12-417011-7.00003-9.

[8] S. G. R. Salim, E. R. Woolliams, and N. P. Fox, "Calibration of a Photodiode Array Spectrometer Against the Copper Point," *Int. J. Thermophys.*, vol. 35, no. 3–4, pp. 504–515, May 2014, doi: 10.1007/s10765-014-1609-1.

[9] V. Vabson *et al.*, "Laboratory Intercomparison of Radiometers Used for Satellite Validation in the 400–900 nm Range," *Remote Sens.*, vol. 11, no. 9, p. 1101, Jan. 2019, doi: 10.3390/rs11091101.

[10] V. Vabson *et al.*, "Field Intercomparison of Radiometers Used for Satellite Validation in the 400–900 nm Range," *Remote Sens.*, vol. 11, no. 9, p. 1129, Jan. 2019, doi: 10.3390/rs11091129.

[11] O. Burggraaff, "Biases from incorrect reflectance convolution," *Opt. Express*, vol. 28, no. 9, pp. 13801–13816, Apr. 2020, doi: 10.1364/OE.391470.

[12] M. Talone, G. Zibordi, I. Ansko, A. C. Banks, and J. Kuusk, "Stray light effects in above-water remote-sensing reflectance from hyperspectral radiometers," *Appl. Opt.*, vol. 55, no. 15, pp. 3966–3977, May 2016, doi: 10.1364/AO.55.003966.

[13] J. Kuusk, I. Ansko, A. Bialek, R. Vendt, and N. Fox, "Implication of Illumination Beam Geometry on Stray Light and Bandpass Characteristics of Diode Array Spectrometer," *IEEE J. Sel. Top. Appl. Earth Obs. Remote Sens.*, vol. 11, no. 8, pp. 2925–2932, Aug. 2018, doi: 10.1109/JSTARS.2018.2841772.

[14] T. Pulli, P. Kärhä, and E. Ikonen, "A method for optimizing the cosine response of solar UV diffusers," *J. Geophys. Res. Atmospheres*, vol. 118, no. 14, pp. 7897–7904, 2013, doi: 10.1002/jgrd.50642.

[15] T. Pulli, P. Kärhä, J. Mes, J. Schreder, P. Jaanson, and F. Manoocheri, "Improved diffusers for solar UV spectroradiometers," *AIP Conf. Proc.*, vol. 1531, no. 1, pp. 813–816, May 2013, doi: 10.1063/1.4804894.

[16] C. P. Ball *et al.*, "Effect of polytetrafluoroethylene (PTFE) phase transition at 19°C on the use of Spectralon as a reference standard for reflectance," *Appl. Opt.*, vol. 52, no. 20, pp. 4806–4812, Jul. 2013, doi: 10.1364/AO.52.004806.

[17] "Satlantic Instrument File Standard Satlantic's Data Format Standard for calibration and Telemetry Definition Files SAT-DN-00134, Ver 6.1, 02/04/2010." Satlantic, 2010.

11 Acknowledgement

This work has made use of the laboratory facilities of Tartu Observatory, University of Tartu also funded by the Estonian Research Council project TT8 and the Estonian State Shared Service Center project KosEST.